Appl. Math. Mech. -Engl. Ed., **42**(8), 1135–1154 (2021)

APPLIED MATHEMATICS AND MECHANICS (ENGLISH EDITION)

https://doi.org/10.1007/s10483-021-2757-6

Vibration absorption of parallel-coupled nonlinear energy sink under shock and harmonic excitations*

Jian'en CHEN[1,2,†], Wei ZHANG[3], Jun LIU[1,2], Wenhua HU[1,2]

1. Tianjin Key Laboratory for Advanced Mechatronic System Design and Intelligent Control, School of Mechanical Engineering, Tianjin University of Technology, Tianjin 300384, China;
2. National Demonstration Center for Experimental Mechanical and Electrical Engineering Education, Tianjin University of Technology, Tianjin 300384, China;
3. Beijing Key Laboratory of Nonlinear Vibrations and Strength of Mechanical Structures, College of Mechanical Engineering, Beijing University of Technology, Beijing 100124, China

(Received Apr. 13, 2021 / Revised May 30, 2021)

Abstract Nonlinear energy sink (NES) can passively absorb broadband energy from primary oscillators. Proper multiple NESs connected in parallel exhibit superior performance to single-degree-of-freedom (SDOF) NESs. In this work, a linear coupling spring is installed between two parallel NESs so as to expand the application scope of such vibration absorbers. The vibration absorption of the parallel and parallel-coupled NESs and the system response induced by the coupling spring are studied. The results show that the responses of the system exhibit a significant difference when the heavier cubic oscillators in the NESs have lower stiffness and the lighter cubic oscillators have higher stiffness. Moreover, the efficiency of the parallel-coupled NES is higher for medium shocks but lower for small and large shocks than that of the parallel NESs. The parallel-coupled NES also shows superior performance for medium harmonic excitations until higher response branches are induced. The performance of the parallel-coupled NES and the SDOF NES is compared. It is found that, regardless of the chosen SDOF NES parameters, the performance of the parallel-coupled NES is similar or superior to that of the SDOF NES in the entire force range.

Key words coupling influence, nonlinear energy sink (NES), vibration absorption

Chinese Library Classification O327
2010 Mathematics Subject Classification 74H45

* Citation: CHEN, J. E., ZHANG, W., LIU, J., and HU, W. H. Vibration absorption of parallel-coupled nonlinear energy sink under shock and harmonic excitations. *Applied Mathematics and Mechanics* (*English Edition*), **42**(8), 1135–1154 (2021) https://doi.org/10.1007/s10483-021-2757-6

† Corresponding author, E-mail: vchenje@163.com

Project supported by the National Natural Science Foundation of China (Nos. 11872274 and 11702188) and the Tianjin Natural Science Foundation of China (No. 18JCYBJC19900)

1 Introduction

Nonlinear energy sink (NES) can engage in resonance with modes over broad frequency bands because of lacking a preferential resonant frequency. Therefore, broadband energy can be effectively transferred from primary systems to properly designed NESs[1–3]. Due to this advantage, NESs are being widely used in a wide variety of engineering applications. In order to meet the engineering requirements, several novel devices based on the theory of targeted energy transfer are proposed. Among those, vibro-impact NES[4–6] is the least like original design of purely cubic stiffness absorber. It consumes energy through the impact between the primary system and an internal impactor, and can be connected in parallel with cubic NES to enhance energy absorption[7–8]. Rotary-oscillatory NES is capable of dissipating energy with its angular and radial damping elements[9]. Piecewise linear stiffness NES is straightforward to manufacture, and can effectively transfer energy[10–12]. NES with piecewise quadratic damping[13] and non-smooth NES with descending stiffness[14] can suppress high branches of response within a given range of excitation amplitude.

Magnetic components were used to realize purely cubic stiffness instead of springs and strings, which enable the design of cubic NES to be more flexible[15–16]. It was shown that the shock mitigation performance of asymmetric magnet-based NES is superior to that of symmetric stiffness-based NES[17]. Bi-stable and multi-stable components[18–20] as well as internal rotators[21–22] and inerters[23–25] were used to transfer energy and improve the vibration absorption performance.

Several traditional cubic NESs can be connected in series or parallel so as to improve the vibration absorption performance. Multiple-degree-of-freedom cubic NESs in series have been investigated[26–28], and it was shown that they have superior performance with respect to single-degree-of-freedom (SDOF) NESs of equal mass[29–31]. Cubic NESs in parallel[32–34] have been also found to have superior performance with respect to SDOF NESs, and have simpler structure than NESs in series.

The historical progress of NES is reviewed in detail from the viewpoints of design, analysis, and application, respectively[35]. The properties and improvement of NES still attract much attention. NiTiNOL-steel wire ropes are used to enhance the performance of cubic NES[36]. The vibration reduction of the multiple modes of a cantilever beam is investigated by using an impact damper[37]. The vibration absorption of a cubic NES under harmonic and random base excitations is studied[38].

With the development of dynamical theory and design methods, NES has been considering in a growing number of engineering applications. Existing research shows that the vibrations of engine crankshaft[39], rotor system[40], hypersonic wing[41], whole spacecraft[42], fluid conveying pipes[43–44], and composite laminated plate[45] can be effectively suppressed by NES. NES is used to integrate with a viscoelastic isolation system[46] to improve its performance and a piezoelectric device[47] to realize vibration reduction and broad-band energy harvest simultaneously. It can also be used to mitigate seismic response and applied in civil engineering[48–51]. In some cases, the excitations imposed on the primary system are known in advance and/or only changed in a small range. Therefore, NES can be optimized and compared in a straightforward manner. However, in certain other cases, when the excitations are unknown and/or vary over a wide range, e.g., the seismic load of buildings and the combined load for aircrafts and spacecrafts, the development of NES must balance the vibration absorption influence of both small and large excitations.

In this work, a linear spring is attached to two traditional cubic NESs in parallel to construct parallel-coupled NES with favorable performance over a large range of excitations. We aim to enhance the performance of the NES as much as possible through a minor change of the existing design. In Sections 2 and 3, the vibration absorption of the parallel-coupled NES is studied and the variation in the dynamic response of the system induced by the coupling spring is analyzed.

In Section 4, the performance of the parallel-coupled NES and an SDOF cubic NES is compared under shock and harmonic excitations. In Section 5, the main conclusions are summarized.

2 Coupling influence under shock excitation

Figure 1 shows a linear primary oscillator attached to two parallel purely cubic oscillators connected by a linear spring. M, μ, and K represent the mass, damping, and stiffness of the linear oscillator, respectively. $m_{1,2}$, $\lambda_{1,2}$, and $k_{1,2}$ are the mass, damping, and stiffness of the two cubic oscillators, respectively. k_3 is the stiffness of the linear coupling spring. F is the external force. The two cubic oscillators are referred to as the parallel NESs for $k_3 = 0$, and the integrated absorber is referred to as the parallel-coupled NES for $k_3 \neq 0$.

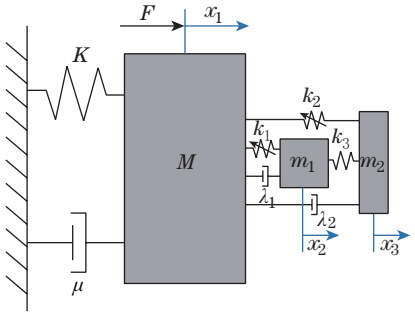

Fig. 1 Linear primary oscillator attached to the parallel-coupled NES

The dynamic equations of the linear primary oscillator attached to the parallel-coupled NES are derived as follows:

$$M\ddot{x}_1 + \mu\dot{x}_1 + Kx_1 + \lambda_1(\dot{x}_1 - \dot{x}_2) + k_1(x_1 - x_2)^3 + \lambda_2(\dot{x}_1 - \dot{x}_3) + k_2(x_1 - x_3)^3 = F, \tag{1a}$$

$$m_1\ddot{x}_2 + \lambda_1(\dot{x}_2 - \dot{x}_1) + k_1(x_2 - x_1)^3 + k_3(x_2 - x_3) = 0, \tag{1b}$$

$$m_2\ddot{x}_3 + \lambda_2(\dot{x}_3 - \dot{x}_1) + k_2(x_3 - x_1)^3 + k_3(x_3 - x_2) = 0, \tag{1c}$$

where the overdot represents the derivative with respect to time. Then, the following parameters are introduced:

$$\begin{cases} \varepsilon_1 = \dfrac{m_1}{M}, \quad \varepsilon_2 = \dfrac{m_2}{M}, \quad \widetilde{t} = \sqrt{\dfrac{K}{M}}t, \quad \widetilde{\mu} = \dfrac{\mu}{\sqrt{KM}}, \quad \widetilde{\lambda}_1 = \dfrac{\lambda_1}{\sqrt{KM}}, \\ \widetilde{\lambda}_2 = \dfrac{\lambda_2}{\sqrt{KM}}, \quad \widetilde{F} = \dfrac{F}{K}, \quad \widetilde{k}_1 = \dfrac{k_1}{K}, \quad \widetilde{k}_2 = \dfrac{k_2}{K}, \quad \widetilde{k}_3 = \dfrac{k_3}{K}. \end{cases}$$

Using the above transformations, Eq. (1) is rewritten as

$$\ddot{x}_1 + \widetilde{\mu}\dot{x}_1 + x_1 + \widetilde{\lambda}_1(\dot{x}_1 - \dot{x}_2) + \widetilde{k}_1(x_1 - x_2)^3 + \widetilde{\lambda}_2(\dot{x}_1 - \dot{x}_3) + \widetilde{k}_2(x_1 - x_3)^3 = \widetilde{F}, \tag{2a}$$

$$\varepsilon_1\ddot{x}_2 + \widetilde{\lambda}_1(\dot{x}_2 - \dot{x}_1) + \widetilde{k}_1(x_2 - x_1)^3 + \widetilde{k}_3(x_2 - x_3) = 0, \tag{2b}$$

$$\varepsilon_2\ddot{x}_3 + \widetilde{\lambda}_2(\dot{x}_3 - \dot{x}_1) + \widetilde{k}_2(x_3 - x_1)^3 + \widetilde{k}_3(x_3 - x_2) = 0. \tag{2c}$$

First, we investigate the influence of the coupling spring on the system response under shock excitation. The Runge-Kutta method is used to solve Eq. (2). For convenience, the overbars of

the dimensionless parameters in the following analysis are dropped. The primary oscillator is excited by the following half-wave shock:

$$F = \begin{cases} f\sin(2\pi t/T), & 0 \leqslant t \leqslant T/2, \\ 0, & t > T/2, \end{cases} \tag{3}$$

where $T = 0.4/\pi$.

The total energy of the primary oscillator is

$$E_{1,2} = \frac{1}{2}\int_0^t (x_1^2 + \dot{x}_1^2)\mathrm{d}\tau.$$

The vibration absorption efficiency is

$$\eta = \frac{E_1 - E_2}{E_1},$$

where E_1 represents the total energy of the primary oscillator without an NES attached, and E_2 represents the total energy of the primary oscillator attached to a given NES.

The vibration absorption efficiency of the parallel and parallel-coupled NESs is shown in Fig. 2. The following parameters are chosen:

$$\varepsilon_1 = 0.07, \quad \varepsilon_2 = 0.03, \quad \lambda_1 = 0.007, \quad \lambda_2 = 0.003, \quad k_1 = 0.1, \quad k_2 = 0.5.$$

It is noted that the two cubic oscillators have different parameters and the heavier cubic oscillator has higher damping and lower stiffness for both the parallel NESs and the parallel-coupled NES. Figure 2 shows that the parallel NESs are activated for a small excitation. However, its efficiency quickly drops with the increase in the excitation. At $f = 11$, the efficiency returns to a high value. The efficiency curve of the parallel-coupled NES is smoother with respect to that of the parallel NESs. The latter rises rapidly from $f = 5$, and reaches its peak at $f = 9$. It is seen that the efficiency of the parallel-coupled NES is higher than that of the parallel NESs for medium excitations. However, it is lower for both small and large excitations. It can be concluded that both the parallel and parallel-coupled NESs have their respective advantages.

In order to elucidate the reason for the occurrence of the two peaks in the efficiency of the parallel NESs, the waveforms of the system are shown in Figs. 3–5.

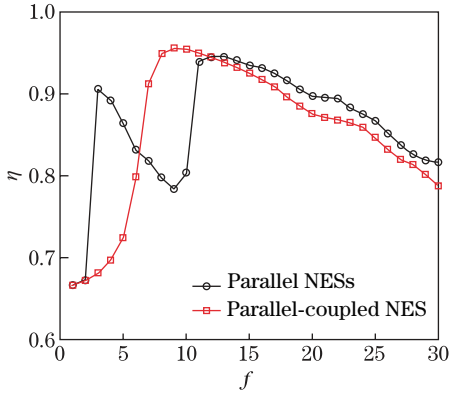

Fig. 2 Vibration absorption efficiency of the parallel ($k_3 = 0$) and parallel-coupled ($k_3 = 0.1$) NESs with shock amplitude, where $\varepsilon_1 = 0.07$, $\varepsilon_2 = 0.03$, $\lambda_1 = 0.007$, $\lambda_2 = 0.003$, $k_1 = 0.1$, and $k_2 = 0.5$ (color online)

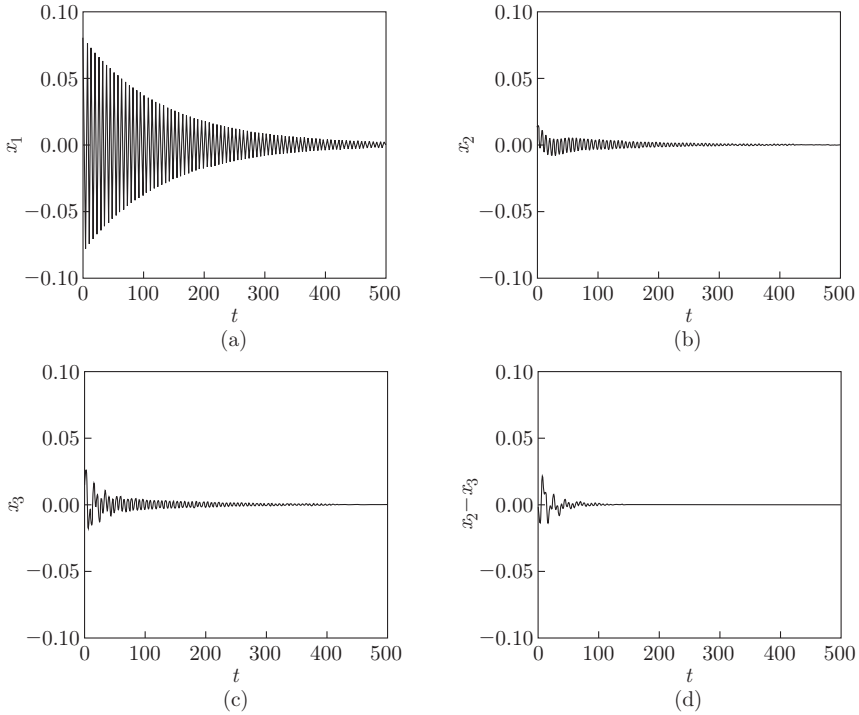

Fig. 3 Responses of the system with the parallel NESs at $f = 2$

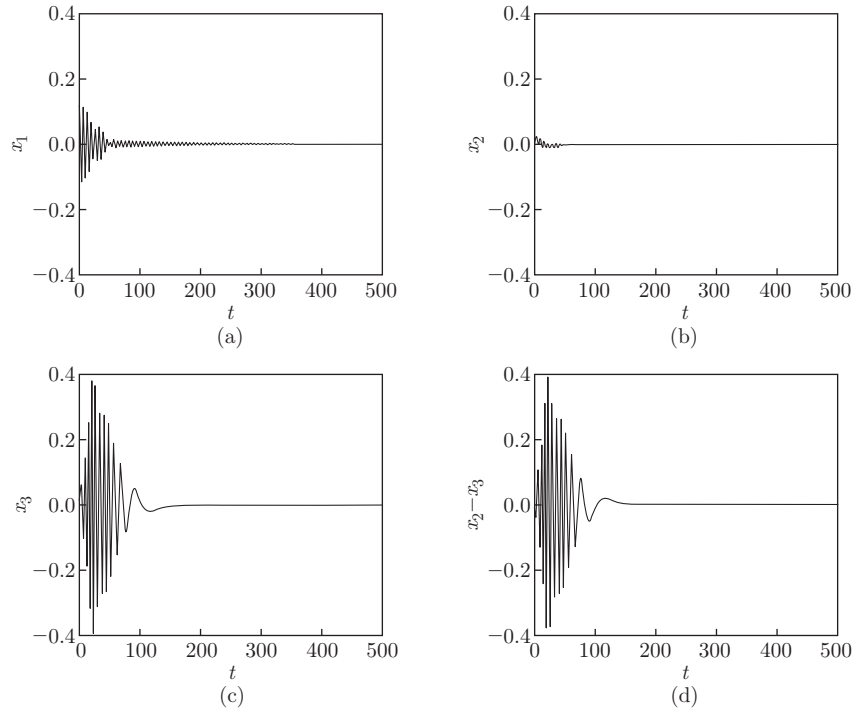

Fig. 4 Responses of the system with the parallel NESs at $f = 3$

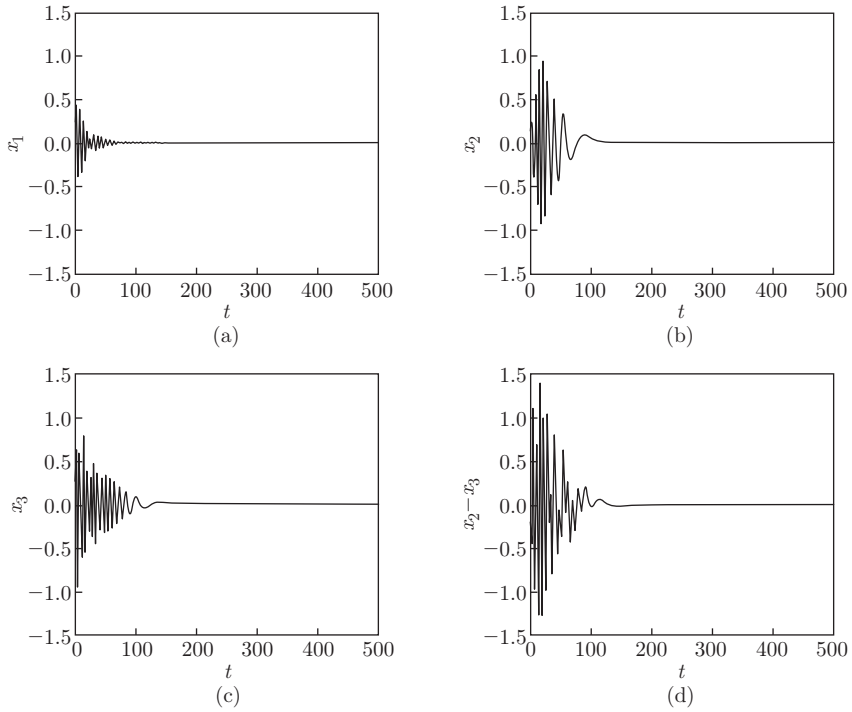

Fig. 5 Responses of the system with the parallel NESs at $f = 11$

At $f = 2$, the amplitudes of the two cubic oscillators of the parallel NESs are both relatively small, and thus the vibration of the primary oscillator is prolonged. The vibrations of the two cubic oscillators are different because of the difference of their parameters. At $f = 3$, the lighter cubic oscillators undergo a large amplitude vibration. However, the amplitude of the other one remains low. A large amount of energy of the primary oscillator is dissipated due to the activation of one of the NESs, causing the efficiency of the parallel NESs to reach the first peak. Since the motion of the two oscillators in the parallel NESs is relatively independent, the obtained result is in accord with that of the SDOF NES, i.e., NES with small mass and/or large stiffness is easier to activate. At $f = 11$, the two cubic oscillators are both activated and produce large amplitude vibrations, causing the efficiency of the parallel NESs to reach its second peak. Generally, an SDOF NES with large mass and/or small stiffness has higher efficiency under large shocks. Therefore, these parallel NESs can be activated under small shocks and have excellent performance under larger shocks. However, the efficiency for medium shocks is not favorable.

The waveforms of the system with the parallel-coupled NES are shown in Figs. 6 and 7. The responses of the primary oscillator with the parallel and parallel-coupled NESs are almost the same at $f = 2$. The responses of the two cubic oscillators in the parallel-coupled NES are similar due to the elastic connection between them. However, the case is different when the two cubic oscillators are both activated. The relative motion between the two cubic oscillators in the parallel NESs is significantly larger than that in the parallel-coupled NES. However, the relative motion in the parallel NESs has no practical significance for vibration absorption. Moreover, the efficiency of the parallel-coupled NES is slightly higher than that of the parallel NESs, and the amplitudes of the two cubic oscillators in the parallel and parallel-coupled NESs are close. Therefore, it can be concluded that the phase difference of the two cubic oscillators in the parallel-coupled NES is smaller than that in the parallel NESs due to linear coupling.

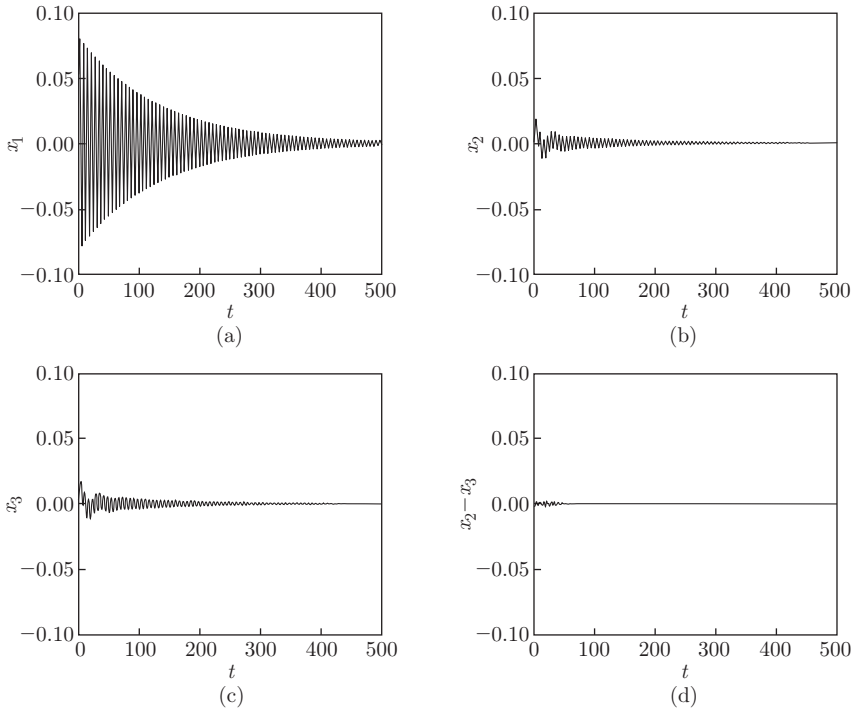

Fig. 6 Responses of the system with the parallel-coupled NES at $f = 2$

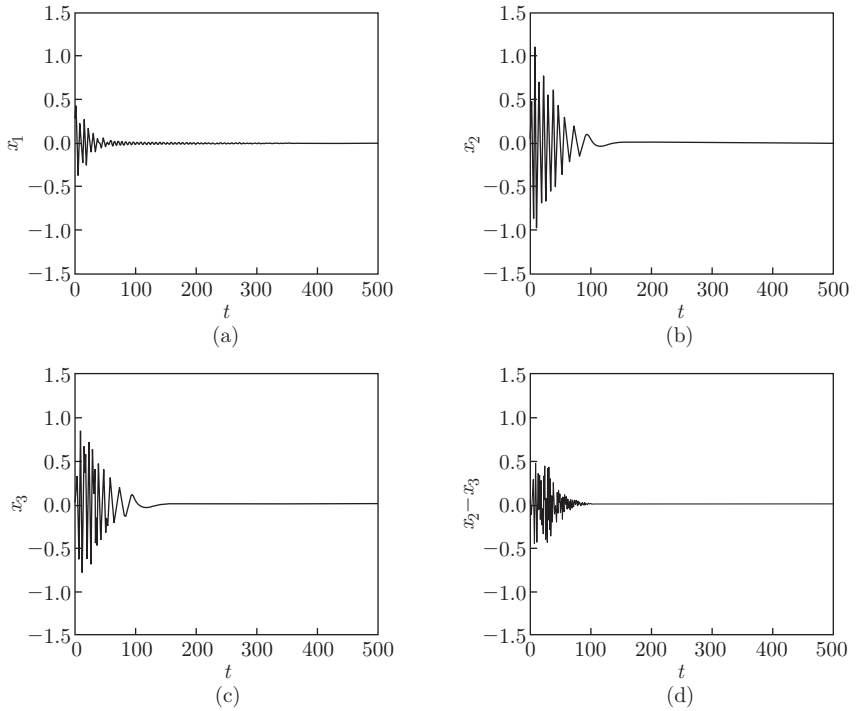

Fig. 7 Responses of the system with the parallel-coupled NES at $f = 11$

The influence of the stiffness of the connection spring is shown in Fig. 8. With the increase in k_3, the activating force of the parallel-coupled NES is reduced. However, the efficiency for large excitations is also reduced. The further increase in the coupling stiffness slightly enhances the efficiency under small shocks but greatly reduces the efficiency under large shocks when the stiffness reaches a certain value.

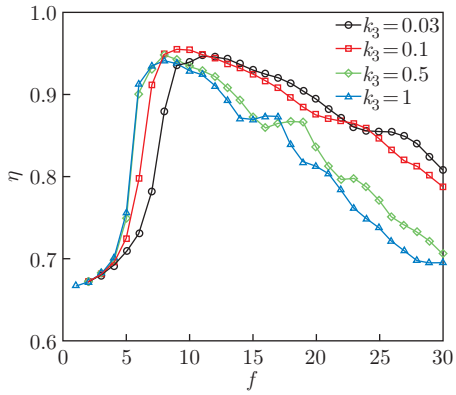

Fig. 8 Influence of the coupling spring stiffness on the vibration absorption efficiency of the parallel-coupled NES, where $\varepsilon_1 = 0.07$, $\varepsilon_2 = 0.03$, $\lambda_1 = 0.007$, $\lambda_2 = 0.003$, $k_1 = 0.1$, and $k_2 = 0.5$ (color online)

The influence of the distributions of mass and damping is shown in Fig. 9. The total mass and damping are kept unchanged, and the mass ratio of the cubic oscillators is equal to their damping ratio. We define the ratio of ε_1 to ε_2 over the ratio of k_1 to k_2 as the degree of asymmetry. It can be concluded that with the reduction of the degree of asymmetry, both the activating force and the efficiency for large shocks decrease and the influence of the change in the degree of asymmetry and the coupling stiffness is similar.

Figure 10 shows the comparison of the efficiency of the parallel and parallel-coupled NESs with the same degree of asymmetry. It is shown that, with the reduction in the degree of

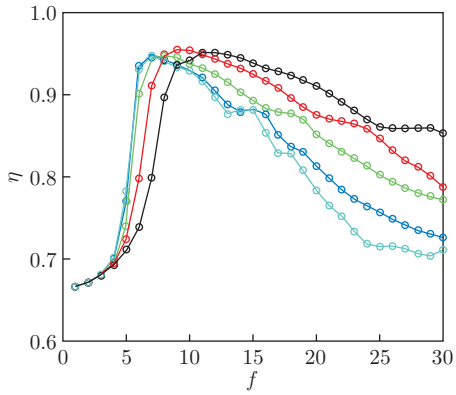

Fig. 9 Influence of the distributions of mass and damping on the vibration absorption efficiency of the parallel-coupled NES, where $k_1 = 0.1$, $k_2 = 0.5$, and $k_3 = 0.1$. Black curve: $\varepsilon_1 = 0.09$, $\varepsilon_2 = 0.01$, $\lambda_1 = 0.009$, and $\lambda_2 = 0.001$. Red curve: $\varepsilon_1 = 0.07$, $\varepsilon_2 = 0.03$, $\lambda_1 = 0.007$, and $\lambda_2 = 0.003$. Green curve: $\varepsilon_1 = 0.05$, $\varepsilon_2 = 0.05$, $\lambda_1 = 0.005$, and $\lambda_2 = 0.005$. Blue curve: $\varepsilon_1 = 0.03$, $\varepsilon_2 = 0.07$, $\lambda_1 = 0.003$, and $\lambda_2 = 0.007$. Cyan curve: $\varepsilon_1 = 0.01$, $\varepsilon_2 = 0.09$, $\lambda_1 = 0.001$, and $\lambda_2 = 0.009$ (color online)

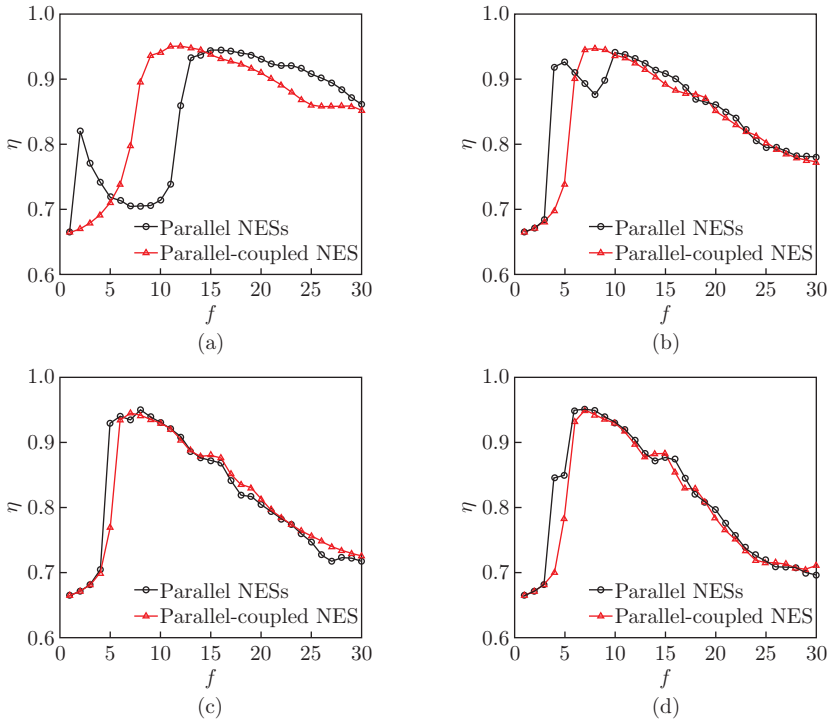

Fig. 10 Comparison of efficiency between the parallel ($k_3 = 0$) and parallel-coupled ($k_3 = 0.1$) NESs, where $k_1 = 0.1$, and $k_2 = 0.5$. (a) $\varepsilon_1 = 0.09$, $\varepsilon_2 = 0.01$, $\lambda_1 = 0.009$, and $\lambda_2 = 0.001$. (b) $\varepsilon_1 = 0.05$, $\varepsilon_2 = 0.05$, $\lambda_1 = 0.005$, and $\lambda_2 = 0.005$. (c) $\varepsilon_1 = 0.03$, $\varepsilon_2 = 0.07$, $\lambda_1 = 0.003$, and $\lambda_2 = 0.007$. (d) $\varepsilon_1 = 0.01$, $\varepsilon_2 = 0.09$, $\lambda_1 = 0.001$, and $\lambda_2 = 0.009$ (color online)

asymmetry, the difference between the efficiency of the two kinds of NESs becomes smaller and smaller. In Figs. 10(c) and (d), the black and red curves almost overlap under large shocks. However, Fig. 10(a) shows a difference between the two curves that exceeds the one in Fig. 2. The light cubic oscillator in the parallel NESs can be activated with a smaller shock. However, the parallel-coupled NES is superior to the parallel NESs over a wider force range.

3 Coupling influence under harmonic excitation

In this section, we aim at the study on the case of harmonic excitation ($F = f\sin(\Omega t)$). The complexification-averaging method is used to obtain the slow-flow equation of the system. We introduce $v = x_2 - x_3$ and let

$$\dot{x}_1 + \mathrm{i}\Omega x_1 = \alpha_1 \mathrm{e}^{\mathrm{i}\Omega t}, \quad \dot{x}_2 + \mathrm{i}\Omega x_2 = \alpha_2 \mathrm{e}^{\mathrm{i}\Omega t}, \quad \dot{v} + \mathrm{i}\Omega v = \alpha_3 \mathrm{e}^{\mathrm{i}\Omega t}. \tag{4}$$

Subsequently, we obtain the following expressions:

$$\begin{cases} x_1 = \dfrac{\alpha_1 \mathrm{e}^{\mathrm{i}\Omega t} - \bar{\alpha}_1 \mathrm{e}^{-\mathrm{i}\Omega t}}{2\mathrm{i}\Omega}, \quad \dot{x}_1 = \dfrac{\alpha_1 \mathrm{e}^{\mathrm{i}\Omega t} + \bar{\alpha}_1 \mathrm{e}^{-\mathrm{i}\Omega t}}{2}, \\ \ddot{x}_1 = \dfrac{\dot{\alpha}_1 \mathrm{e}^{\mathrm{i}\Omega t} + \mathrm{i}\Omega\alpha_1 \mathrm{e}^{\mathrm{i}\Omega t} + \dot{\bar{\alpha}}_1 \mathrm{e}^{-\mathrm{i}\Omega t} - \mathrm{i}\Omega\bar{\alpha}_1 \mathrm{e}^{-\mathrm{i}\Omega t}}{2}, \end{cases} \tag{5a}$$

$$\begin{cases} x_2 = \dfrac{\alpha_2 \mathrm{e}^{\mathrm{i}\Omega t} - \bar{\alpha}_2 \mathrm{e}^{-\mathrm{i}\Omega t}}{2\mathrm{i}\Omega}, \quad \dot{x}_2 = \dfrac{\alpha_2 \mathrm{e}^{\mathrm{i}\Omega t} + \bar{\alpha}_2 \mathrm{e}^{-\mathrm{i}\Omega t}}{2}, \\ \ddot{x}_2 = \dfrac{\dot{\alpha}_2 \mathrm{e}^{\mathrm{i}\Omega t} + \mathrm{i}\Omega \alpha_2 \mathrm{e}^{\mathrm{i}\Omega t} + \dot{\bar{\alpha}}_2 \mathrm{e}^{-\mathrm{i}\Omega t} - \mathrm{i}\Omega \bar{\alpha}_2 \mathrm{e}^{-\mathrm{i}\Omega t}}{2}, \end{cases} \tag{5b}$$

$$\begin{cases} v = \dfrac{\alpha_3 \mathrm{e}^{\mathrm{i}\Omega t} - \bar{\alpha}_3 \mathrm{e}^{-\mathrm{i}\Omega t}}{2\mathrm{i}\Omega}, \quad \dot{v} = \dfrac{\alpha_3 \mathrm{e}^{\mathrm{i}\Omega t} + \bar{\alpha}_3 \mathrm{e}^{-\mathrm{i}\Omega t}}{2}, \\ \ddot{v} = \dfrac{\dot{\alpha}_3 \mathrm{e}^{\mathrm{i}\Omega t} + \mathrm{i}\Omega \alpha_3 \mathrm{e}^{\mathrm{i}\Omega t} + \dot{\bar{\alpha}}_3 \mathrm{e}^{-\mathrm{i}\Omega t} - \mathrm{i}\Omega \bar{\alpha}_3 \mathrm{e}^{-\mathrm{i}\Omega t}}{2}. \end{cases} \tag{5c}$$

Substituting Eq. (5) into Eq. (2) and retaining the slow-flow parts, we obtain

$$\begin{aligned} &\dot{\alpha}_1 + \mathrm{i}\Omega\alpha_1 + \mu\alpha_1 + \frac{\alpha_1}{\mathrm{i}\Omega} + \lambda_1(\alpha_1 - \alpha_2) \\ &+ \frac{3k_1(\alpha_1 - \alpha_2)^2(\bar{\alpha}_1 - \bar{\alpha}_2)}{4\mathrm{i}\Omega^3} + \lambda_2(\alpha_1 - \alpha_2 + \alpha_3) \\ &+ \frac{3k_2(\alpha_1 - \alpha_2 + \alpha_3)^2(\bar{\alpha}_1 - \bar{\alpha}_2 + \bar{\alpha}_3)}{4\mathrm{i}\Omega^3} = f, \end{aligned} \tag{6a}$$

$$\begin{aligned} &\varepsilon_1(\dot{\alpha}_2 + \mathrm{i}\Omega\alpha_2) + \lambda_1(\alpha_2 - \alpha_1) \\ &+ \frac{3k_1(\alpha_2 - \alpha_1)^2(\bar{\alpha}_2 - \bar{\alpha}_1)}{4\mathrm{i}\Omega^3} + \frac{k_3\alpha_3}{\mathrm{i}\Omega} = 0, \end{aligned} \tag{6b}$$

$$\begin{aligned} &\varepsilon_2(\dot{\alpha}_2 + \mathrm{i}\Omega\alpha_2 - \dot{\alpha}_3 - \mathrm{i}\Omega\alpha_3) + \lambda_2(\alpha_2 - \alpha_3 - \alpha_1) \\ &- \frac{3k_2(\alpha_1 - \alpha_2 + \alpha_3)^2(\bar{\alpha}_1 - \bar{\alpha}_2 + \bar{\alpha}_3)}{4\mathrm{i}\Omega^3} - \frac{k_3\alpha_3}{\mathrm{i}\Omega} = 0. \end{aligned} \tag{6c}$$

Define

$$\alpha_1 = a_1 + \mathrm{i}b_1, \quad \alpha_2 = a_2 + \mathrm{i}b_2, \quad \alpha_3 = a_3 + \mathrm{i}b_3.$$

Then, substituting the above equations into Eq. (6) yields

$$\begin{aligned} &\dot{a}_1 + \mathrm{i}\dot{b}_1 + \mathrm{i}\Omega(a_1 + \mathrm{i}b_1) + \mu(a_1 + \mathrm{i}b_1) \\ &- \frac{\mathrm{i}(a_1 + \mathrm{i}b_1)}{\Omega} + \lambda_1(a_1 + \mathrm{i}b_1 - a_2 - \mathrm{i}b_2) \\ &- \frac{3\mathrm{i}k_1}{4\Omega^3}((a_1 - a_2)^2 + (b_1 - b_2)^2)(a_1 + \mathrm{i}b_1 - a_2 - \mathrm{i}b_2) \\ &+ \lambda_2(a_1 - a_2 + a_3 + \mathrm{i}(b_1 - b_2 + b_3)) - \frac{3\mathrm{i}k_2}{4\Omega^3}((a_1 + a_3 - a_2)^2 \\ &+ (b_1 + b_3 - b_2)^2)(a_1 - a_2 + a_3 + \mathrm{i}(b_1 + b_3 - b_2)) = f, \end{aligned} \tag{7a}$$

$$\begin{aligned} &\varepsilon_1(\dot{a}_2 + \mathrm{i}\dot{b}_2 + \mathrm{i}\Omega(a_2 + \mathrm{i}b_2)) + \frac{3\mathrm{i}k_1}{4\Omega^3}((a_1 - a_2)^2 \\ &+ (b_1 - b_2)^2)(a_1 + \mathrm{i}b_1 - a_2 - \mathrm{i}b_2) \\ &+ \lambda_1(a_2 + \mathrm{i}b_2 - a_1 - \mathrm{i}b_1) - \frac{\mathrm{i}k_3}{\Omega}(a_3 + \mathrm{i}b_3) = 0, \end{aligned} \tag{7b}$$

$$\varepsilon_2(\dot{a}_2+\mathrm{i}\dot{b}_2+\mathrm{i}\Omega(a_2+\mathrm{i}b_2)-\dot{a}_3-\mathrm{i}\dot{b}_3-\mathrm{i}\Omega(a_3+\mathrm{i}b_3))$$
$$+\lambda_2(a_2-a_3-a_1+\mathrm{i}(b_2-b_3-b_1))$$
$$+\frac{3\mathrm{i}k_2}{4\Omega^3}((a_1-a_2+a_3)^2+(b_1-b_2+b_3)^2)(a_1-a_2+a_3+\mathrm{i}(b_1-b_2+b_3))$$
$$+\frac{\mathrm{i}k_3}{\Omega}(a_3+\mathrm{i}b_3)=0. \tag{7c}$$

Separating the real and imaginary parts of Eq. (7) yields

$$\dot{a}_1=\Omega b_1-\frac{b_1}{\Omega}-\mu a_1-\lambda_1(a_1-a_2)-\frac{3k_1}{4\Omega^3}((a_1-a_2)^2$$
$$+(b_1-b_2)^2)(b_1-b_2)-\lambda_2(a_1+a_3-a_2)$$
$$-\frac{3k_2}{4\Omega^3}((a_1+a_3-a_2)^2+(b_1+b_3-b_2)^2)(b_1+b_3-b_2)+f, \tag{8a}$$

$$\dot{b}_1=-\Omega a_1+\frac{a_1}{\Omega}-\mu b_1-\lambda_1(b_1-b_2)+\frac{3k_1}{4\Omega^3}((a_1-a_2)^2$$
$$+(b_1-b_2)^2)(a_1-a_2)-\lambda_2(b_1+b_3-b_2)+\frac{3k_2}{4\Omega^3}((a_1+a_3-a_2)^2$$
$$+(b_1+b_3-b_2)^2)(a_1+a_3-a_2), \tag{8b}$$

$$\dot{a}_2=\Omega b_2-\frac{\lambda_1}{\varepsilon_1}(a_2-a_1)-\frac{k_3}{\Omega\varepsilon_1}b_3+\frac{3k_1}{4\varepsilon_1\Omega^3}((a_1-a_2)^2+(b_1-b_2)^2)(b_1-b_2), \tag{8c}$$

$$\dot{b}_2=-\Omega a_2-\frac{\lambda_1}{\varepsilon_1}(b_2-b_1)+\frac{k_3}{\Omega\varepsilon_1}a_3-\frac{3k_1}{4\varepsilon_1\Omega^3}((a_1-a_2)^2+(b_1-b_2)^2)(a_1-a_2), \tag{8d}$$

$$\varepsilon_2(\dot{a}_2-\Omega b_2-\dot{a}_3+\Omega b_3)+\lambda_2(a_2-a_3-a_1)-\frac{k_3b_3}{\Omega}$$
$$-\frac{3k_2}{4\Omega^3}((a_1-a_2+a_3)^2+(b_1-b_2+b_3)^2)(b_1+b_3-b_2)=0, \tag{8e}$$

$$\varepsilon_2(\dot{b}_2+\Omega a_2-\dot{b}_3-\Omega a_3)+\lambda_2(b_2-b_3-b_1)+\frac{k_3a_3}{\Omega}$$
$$+\frac{3k_2}{4\Omega^3}((a_1-a_2+a_3)^2+(b_1-b_2+b_3)^2)(a_1+a_3-a_2)=0. \tag{8f}$$

Substituting Eqs. (8c) and (8d) into Eqs. (8e) and (8f), we obtain

$$\dot{a}_3=-\frac{\lambda_1}{\varepsilon_1}(a_2-a_1)-\frac{k_3}{\Omega}\Big(\frac{1}{\varepsilon_1}+\frac{1}{\varepsilon_2}\Big)b_3+\frac{3k_1}{4\varepsilon_1\Omega^3}((a_1-a_2)^2$$
$$+(b_1-b_2)^2)(b_1-b_2)+\Omega b_3+\frac{\lambda_2}{\varepsilon_2}(a_2-a_3-a_1)$$
$$-\frac{3k_2}{4\varepsilon_2\Omega^3}((a_1-a_2+a_3)^2+(b_1-b_2+b_3)^2)(b_1+b_3-b_2), \tag{9a}$$

$$\dot{b}_3 = -\frac{\lambda_1}{\varepsilon_1}(b_2 - b_1) + \frac{k_3}{\Omega}\Big(\frac{1}{\varepsilon_1} + \frac{1}{\varepsilon_2}\Big)a_3 - \frac{3k_1}{4\varepsilon_1\Omega^3}((a_1 - a_2)^2 + (b_1 - b_2)^2)(a_1 - a_2) - \Omega a_3$$
$$+ \frac{\lambda_2}{\varepsilon_2}(b_2 - b_3 - b_1) + \frac{3k_2}{4\varepsilon_2\Omega^3}((a_1 - a_2 + a_3)^2 + (b_1 - b_2 + b_3)^2)(a_1 + a_3 - a_2). \quad (9b)$$

In the above equations, $\dot{a}_1$, $\dot{b}_1$, $\dot{a}_2$, $\dot{b}_2$, $\dot{a}_3$, and $\dot{b}_3$ are set to zero in order to obtain the steady-state solutions. A represents the response amplitude of the primary oscillator, and is given by $A = \frac{\sqrt{a_1^2+b_1^2}}{\Omega}$.

In order to verify the derivation, the result obtained by the complexification-averaging method is compared with that obtained by the Runge-Kutta method which is used to directly solve Eq. (2). Figure 11 shows the frequency responses at $f = 0.002$ and the slow-flow equation is solved with a code based on the least square method. The stability of the steady-state solutions is obtained from the eigenvalues of the Jacobian matrix of Eqs. (8a)–(8d) and (9). The results obtained from the two methods are found to be in good agreement. The parameters in Figs. 11–16 are the same as those in Fig. 2.

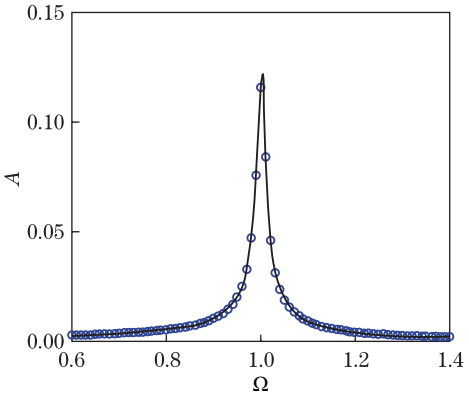

Fig. 11 Comparison of the complexification-averaging method and the Runge-Kutta method (frequency responses of the primary oscillator attached to the parallel-coupled NES at $f = 0.002$) (color online)

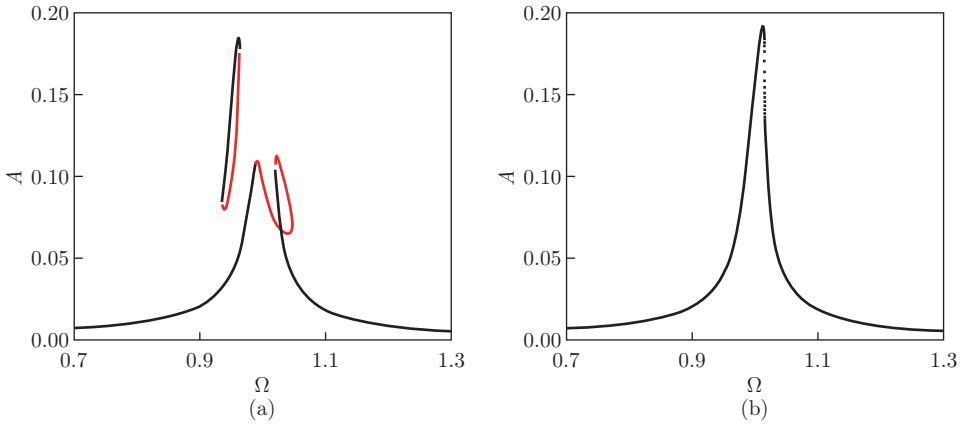

Fig. 12 Frequency responses of the primary oscillator at $f = 0.004$ with the (a) parallel and (b) parallel-coupled NESs, where black points represent the stable responses and red points represent the unstable responses (color online)

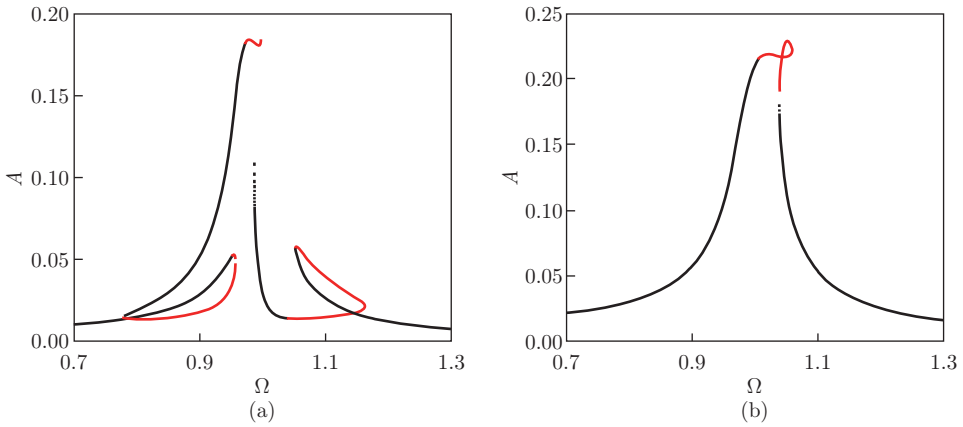

Fig. 13 Frequency responses of the primary oscillator at $f = 0.011$ with the (a) parallel and (b) parallel-coupled NESs, where black points represent the stable responses and red points represent the unstable responses (color online)

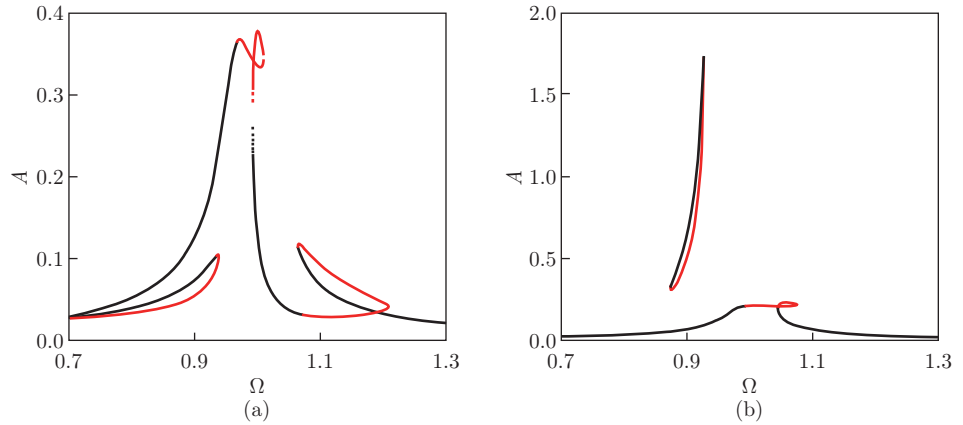

Fig. 14 Frequency responses of the primary oscillator at $f = 0.014$ with the (a) parallel and (b) parallel-coupled NESs, where black points represent the stable responses and red points represent the unstable responses (color online)

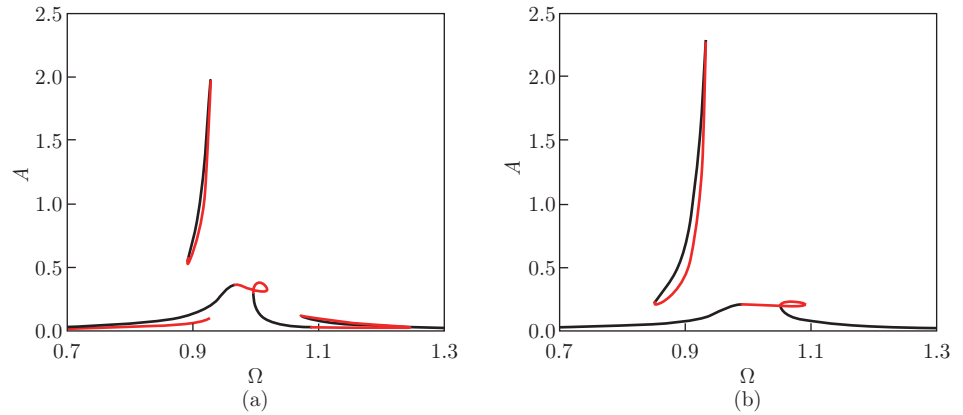

Fig. 15 Frequency responses of the primary oscillator at $f = 0.016$ with the (a) parallel and (b) parallel-coupled NESs, where black points represent the stable responses and red points represent the unstable responses (color online)

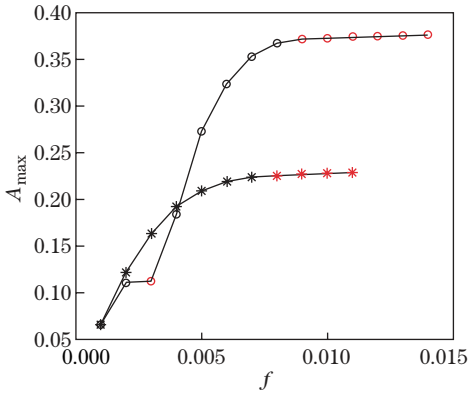

Fig. 16 Dependence of the maximal amplitude of the primary oscillator on the excitation amplitude. Black and red circles: stable and unstable responses of the primary oscillator attached to the parallel NESs. Black and red asterisks: stable and unstable responses of the primary oscillator attached to the parallel-coupled NES (color online)

Figures 12–15 show the variations in responses of the primary oscillator attached to different NESs. The system with the parallel NESs generates higher branches of responses at $f = 0.004$ in a frequency band that is slightly lower than the linear natural frequency of the primary oscillator. For periodic excitations imposed on the system, higher stable branches of responses can occur for specific initial conditions in the simulation as well as for certain external conditions in practical engineering. Under this force, the response of the primary oscillator with the parallel-coupled NES is like the response of a linear system, and its peak value is moderately higher. For excitation amplitude at $f = 0.011$, the higher and lower branches of the former system merge. However, the latter system still has only the lower branch. Unstable responses in narrow frequency bands can be seen in two subfigures of Fig. 13, and these unstable responses in most cases manifest as strongly modulated responses. The peak value in the former system is markedly larger than that in the latter.

For the excitation amplitude at $f = 0.014$, the amplitude in the former system slightly increases with respect to the case of $f = 0.011$. In the latter system, the higher branches of responses are present, and therefore the peak value increases several times. At $f = 0.016$, the peak value in the latter system exhibits only a minor increase with respect to that in Fig. 14(b). It can be concluded based on Figs. 13–15 that once the higher branches are present, the amplitudes of both systems increase slowly with the increase in excitation forcing. However, the higher branches of responses occur again in the former system, and the peak value dramatically increases. For the parallel-coupled NES, the higher branches only occur once, owing to the connection between two cubic oscillators. Since the parameters of the two cubic oscillators of the parallel NESs significantly differ, the higher branches are induced twice with the increase in the excitation amplitude. Next, the increasing force can affect the evolution of higher branches of responses and lead to merging of higher and lower branches.

Figure 16 shows the comparison of the peak value of the primary oscillator attached to the two different NESs. The performance of the parallel NESs exceeds that of the parallel-coupled NES below $f = 0.004$, while for higher values of f, the converse holds true. When the excitation amplitude further increases, the system with both the parallel-coupled and parallel NESs generate detached higher branches at $f = 0.012$ and $f = 0.015$, respectively. The occurrence of the detached higher branches of responses will significantly reduce the influence of the NESs. It can be considered that the NESs almost lose efficacy once these branches arise. Therefore, only the maximal amplitude of the primary oscillator before higher detached

branches occur is shown. It follows from Fig. 2 that the changes of the vibration absorption performance of both the parallel and parallel-coupled NESs for harmonic excitation are the same as those for shock excitation, i.e., the parallel-coupled NES performs better for medium excitations while the parallel NESs performs better for small and large excitations.

4 Performance comparison with the SDOF NES

Although the influence of the stiffness of the SODF cubic NES on the vibration absorption efficiency is well-known, we still present a figure of this influence for comparing the advantages and disadvantages between this NES and the parallel-coupled NES, as shown in Fig. 17. The system in Eq. (2) can be reduced to a system comprised of a linear primary oscillator and an SDOF NES by letting

$$\lambda_2 = 0, \quad k_2 = 0, \quad k_3 = 0.$$

In accordance with the results shown in Figs. 8 and 9, the SDOF NES with certain parameters and low activating force exhibit lower efficiency for large excitations.

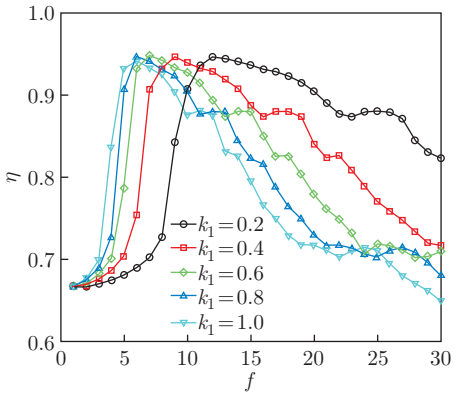

Fig. 17 Influence of the stiffness of the SDOF cubic NES on the vibration absorption efficiency, where $\varepsilon_1 = 0.1$, and $\lambda_1 = 0.01$ (color online)

Figure 18 shows the comparison of the efficiency of the SODF cubic NES and the parallel-coupled NES. It can be seen from Fig. 18(a) that the red curve is above the black curve over the entire force range. Particularly, the efficiency of the parallel-coupled NES with $k_3 = 0.1$ is significantly higher than that of the SDOF NES for large shocks. In addition, the green curve is also above the black curve apart from a few cases. Moreover, the efficiency of the parallel-coupled NES with $k_3 = 0.3$ exhibits superior performance under small shocks. In order to design parallel-coupled NES with superior performance with respect to the SDOF NES, the parameters must be tuned accordingly. In Fig. 18(b), the stiffness of the SDOF NES is set to $k_1 = 0.6$. It is seen that all three curves almost overlap for small shocks, while for large shocks, the red curve is slightly above the black curve while close to the green curve. Many parametric studies were conducted and only several typical cases are shown in this work. The results demonstrate that regardless of the SDOF NES parameters chosen, the parallel-coupled NES with performance close or superior to this SDOF NES can always be constructed across the entire force range.

Figure 19 shows the variation of the peak value of the primary oscillator attached to the SDOF NES with varying stiffness. It is shown that the primary oscillator attached to the NES with higher stiffness has lower peak value for small excitations. However, it is liable to generate higher branches of responses for increasing excitation. Therefore, although

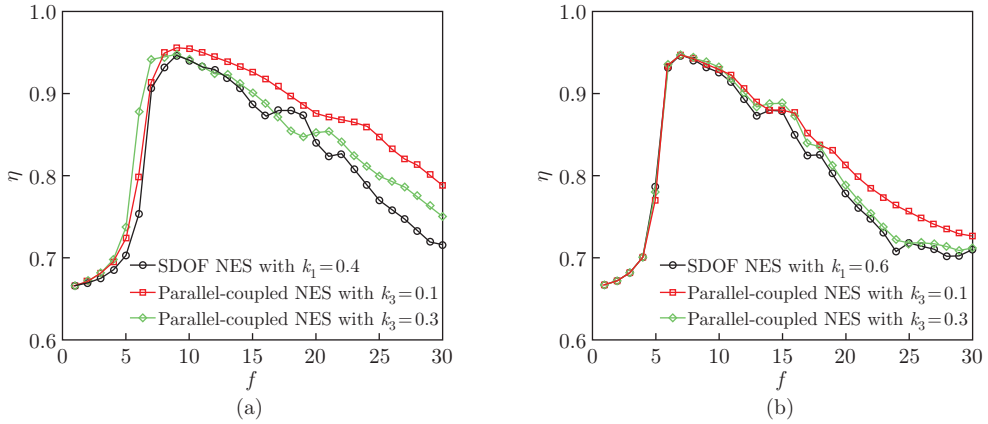

Fig. 18 Comparison of the efficiency between the SDOF cubic NES and the parallel-coupled NES with the parameters of (a) $\varepsilon_1 = 0.07$, $\varepsilon_2 = 0.03$, $\lambda_1 = 0.007$, $\lambda_2 = 0.003$ and (b) $\varepsilon_1 = 0.03$, $\varepsilon_2 = 0.07$, $\lambda_1 = 0.003$, $\lambda_2 = 0.007$ (color online)

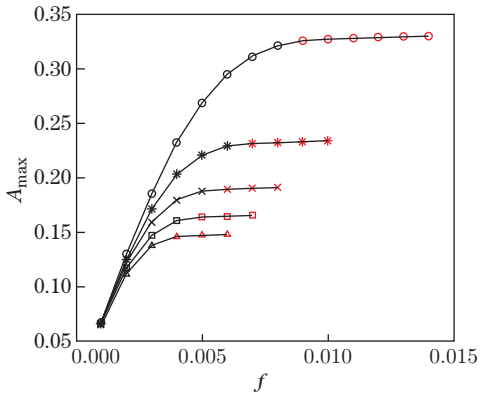

Fig. 19 Influence of the stiffness of the SDOF cubic NES on the maximal amplitude of the primary oscillator, where $\varepsilon_1 = 0.1$, and $\lambda_1 = 0.01$. Black symbols: stable responses. Red symbols: unstable responses. Circles: $k_1 = 0.2$. Asterisks: $k_1 = 0.4$. Crosses: $k_1 = 0.6$. Squares: $k_1 = 0.8$. Triangles: $k_1 = 1$ (color online)

the NES with $k_1 = 0.2$ exhibits the worst performance, the exciting force of higher branches is the largest in this case, indicating the greatest robustness. The responses of the system after higher branches occur are not shown. The performance of the SDOF NES and parallel-coupled NES is compared. The parameters in Figs. 20(a) and 20(b) are the same as those in Figs. 18(a) and 18(b), respectively. The peak values of the system attached to the parallel-coupled NES with two different coupling stiffness are both lower than those of the system attached to the SDOF NES in Fig. 20(a). In addition, the parallel-coupled NES with $k_3 = 0.1$ has larger exciting force of higher branches than the SDOF NES. In Fig. 20(b), the performance of the SDOF NES and parallel-coupled NES is extremely close, and the peak values of the system attached to the parallel-coupled NES are slightly higher than those of the system attached to the SDOF NES. Under the comprehensive consideration of the results in this paper, the performance of the NESs with purely nonlinear stiffness for harmonic excitation can be deduced from the results for shock excitation, and vice versa.

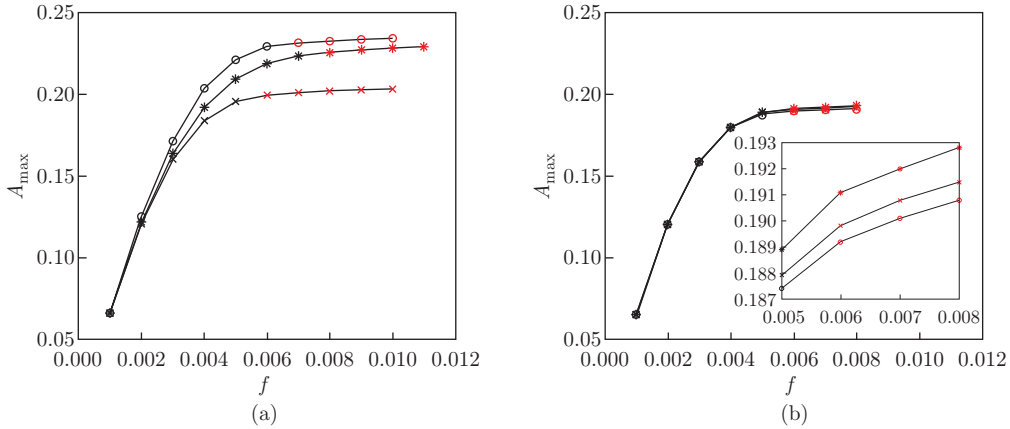

Fig. 20 Comparison of the maximal amplitudes of the primary oscillator attached to the SDOF cubic NES and the parallel-coupled NES, where black symbols indicate the stable responses, and red symbols indicate the unstable responses. (a) Circles, the SDOF NES with $k_1 = 0.4$; asterisks, the parallel-coupled NES with $\varepsilon_1 = 0.07$, $\varepsilon_2 = 0.03$, $\lambda_1 = 0.007$, $\lambda_2 = 0.003$, and $k_3 = 0.1$; crosses, the parallel-coupled NES with $\varepsilon_1 = 0.07$, $\varepsilon_2 = 0.03$, $\lambda_1 = 0.007$, $\lambda_2 = 0.003$, and $k_3 = 0.3$. (b) Circles, the SDOF NES with $k_1 = 0.6$; asterisks, the parallel-coupled NES with $\varepsilon_1 = 0.03$, $\varepsilon_2 = 0.07$, $\lambda_1 = 0.003$, $\lambda_2 = 0.007$, and $k_3 = 0.1$; crosses, the parallel-coupled NES with $\varepsilon_1 = 0.03$, $\varepsilon_2 = 0.07$, $\lambda_1 = 0.003$, $\lambda_2 = 0.007$, and $k_3 = 0.3$ (color online)

5 Conclusions

The parallel-coupled NES is proposed to expand the application range of the purely cubic stiffness absorber, and its performance is studied and compared with the parallel NESs and an SODF NES under shock and harmonic excitations. The Runge-Kutta method, complexification-averaging method, and least square method are used to solve the mathematical model of the system. The principal findings of this study can be stated as follows.

(i) The large response differences of the systems attached to the parallel and parallel-coupled NESs depend not only on the existence of the coupling spring but also on the asymmetric design of the mass and stiffness of the two cubic oscillators.

(ii) The parallel and parallel-coupled NESs have their intrinsic application ranges. The parallel NESs are suitable for the case of both small and large excitations. The parallel-coupled NES is suitable for the case of medium excitations, and its performance for large excitations is also favorable. It should be considered that there are few engineering applications in which only operations with small and large excitations are required.

(iii) The parallel-coupled NES is superior to the SDOF NES across the entire force range in certain parameter ranges, while its performance is close to that of the SDOF NES in the remaining parameter ranges.

References

[1] GEORGIADES, F. and VAKAIS, A. F. Dynamics of a linear beam with an attached local nonlinear energy sink. *Communications in Nonlinear Science and Numerical Simulation*, **12**, 643–651 (2007)

[2] GENDELMAN, O. V. Targeted energy transfer in systems with external and self-excitation. *Proceedings of the Institution of Mechanical Engineers, Part C: Journal of Mechanical Engineering Science*, **225**, 2007–2043 (2011)

[3] KERSCHEN, G., LEE, Y. S., VAKAKIS, A. F., MCFARLAND, D. M., and BERGMAN, L. A. Irreversible passive energy transfer in coupled oscillators with essential nonlinearity. *SIAM Journal on Applied Mathematics*, **66**, 648–679 (2006)

[4] GENDELMAN, O. V. Analytic treatment of a system with a vibro-impact nonlinear energy sink. *Journal of Sound and Vibration*, **331**, 4599–4608 (2012)

[5] GOURC, E., MICHON, G., SEGUY, S., and BERLIOZ, A. Targeted energy transfer under harmonic forcing with a vibro-impact nonlinear energy sink: analytical and experimental developments. *Journal of Vibration and Acoustics*, **137**, 031008 (2015)

[6] LI, T., GOURC, E., SEGUY, S., and BERLIOZ, A. Dynamics of two vibro-impact nonlinear energy sinks in parallel under periodic and transient excitations. *International Journal of Non-Linear Mechanics*, **90**, 100–110 (2017)

[7] NUCERA, F., IACONO, F. L., MCFARLAND, D. M., BERGMAN, L. A., and VAKAKIS, A. F. Application of broadband nonlinear targeted energy transfers for seismic mitigation of a shear frame: experimental results. *Journal of Sound and Vibration*, **313**, 57–76 (2008)

[8] WEI, Y. M., WEI, S., ZHANG, Q. L., DONG, X. J., PENG, Z. K., and ZHANG, W. M. Targeted energy transfer of a parallel nonlinear energy sink. *Applied Mathematics and Mechanics* (*English Edition*), **40**(5), 621–630 (2019) https://doi.org/10.1007/s10483-019-2477-6

[9] SAEED, A. S., AL-SHUDEIFAT, M. A., and VAKAKIS, A. F. Rotary-oscillatory nonlinear energy sink of robust performance. *International Journal of Non-Linear Mechanics*, **117**, 103249 (2019)

[10] GEORGIADES, F., VAKAKIS, A. F., MCFARLAND, D. M., and BERGMAN, L. A. Shock isolation through passive energy pumping caused by nonsmooth nonlinearities. *International Journal of Bifurcation and Chaos*, **15**, 1989–2001 (2005)

[11] GENDELMAN, O. V. Targeted energy transfer in systems with non-polynomial nonlinearity. *Journal of Sound and Vibration*, **315**, 732–745 (2008)

[12] LAMARQUE, C. H., SAVADKOOHI, A. T., CHARLEMAGNE, S., and ABDOULHADI, P. Nonlinear vibratory interactions between a linear and a non-smooth forced oscillator in the gravitational field. *Mechanical System and Signal Processing*, **89**, 131–148 (2017)

[13] STAROSVETSKY, Y. and GENDELMAN, O. V. Vibration absorption in systems with a nonlinear energy sink: nonlinear damping, *Journal of Sound and Vibration*, **324**, 916–939 (2009)

[14] CHEN, J. E., SUN, M., HU, W. H., ZHANG, J. H., and WEI, Z. C. Performance of non-smooth nonlinear energy sink with descending stiffness. *Nonlinear Dynamics*, **100**, 255–267 (2020)

[15] BENACCHIO, S., MALHER, A., BOISSON, J., and TOUZE, C. Design of a magnetic vibration absorber with tunable stiffnesses. *Nonlinear Dynamics*, **85**, 893–911 (2016)

[16] FEUDO, S. L., TOUZE, C., BOISSON, J., and CUMUNEL, G. Nonlinear magnetic vibration absorber for passive control of a multi-storey structure. *Journal of Sound and Vibration*, **438**, 33–53 (2019)

[17] AL-SHUDEIFAT, M. A. Asymmetric magnet-based nonlinear energy sink. *Journal of Computational and Nonlinear Dynamics*, **10**, 014502 (2015)

[18] ROMEO, F., SIGALOV, G., BERGMAN, L. A., and VAKAKIS, A. F. Dynamics of a linear oscillator coupled to a bistable light attachment: numerical study. *Journal of Computational and Nonlinear Dynamics*, **10**, 011007 (2015)

[19] FANG, X., WEN, J. H., YIN, J. F., and YU, D. L. Highly efficient continuous bistable nonlinear energy sink composed of a cantilever beam with partial constrained layer damping. *Nonlinear Dynamics*, **87**, 2677–2695 (2017)

[20] YAO, H. L., WANG, Y. W., CAO, Y. B., and WEN, B. C. Multi-stable nonlinear energy sink for rotor system. *International Journal of Non-Linear Mechanics*, **118**, 103273 (2020)

[21] BENAROUS, N. and GENDELMAN, O. V. Nonlinear energy sink with combined nonlinearities: enhanced mitigation of vibrations and amplitude locking phenomenon. *Proceedings of the Institution of Mechanical Engineers, Part C: Journal of Mechanical Engineering Science*, **230**, 21–33 (2016)

[22] GENDELMAN, O. V., SIGALOV, G., MANEVITCH, L. I., MANE, M., VAKAKIS, A. F., and BERGMAN, L. A. Dynamics of an eccentric rotational nonlinear energy sink. *Journal of Applied Mechanics*, **79**, 011012 (2012)

[23] ZHANG, Y. W., LU, Y. N., ZHANG, W., TENG, Y. Y., YANG, H. X., YANG, T. Z., and CHEN, L. Q. Nonlinear energy sink with inerter. *Mechanical Systems and Signal Processing*, **125**, 52–64 (2019)

[24] JAVIDIALESAADI, A. and WIERSCHEM, N. E. An inerter-enhanced nonlinear energy sink. *Mechanical Systems and Signal Processing*, **129**, 449–454 (2019)

[25] ZHANG, Z., LU, Z. Q., DING, H., and CHEN, L. Q. An inertial nonlinear energy sink. *Journal of Sound and Vibration*, **450**, 199–213 (2019)

[26] TSAKIRTZIS, S., PANAGOPOULOS, P. N., KERSCHEN, G., GENDELMAN, O., VAKAKIS, A. F., and BERGMAN, L. A. Complex dynamics and targeted energy transfer in linear oscillators coupled to multi-degree-of-freedom essentially nonlinear attachments. *Nonlinear Dynamics*, **48**, 285–318 (2007)

[27] WIERSCHEM, N. E., LUO, J., AL-SHUDEIFAT, M., HUBBARD, S., OTT, R., FAHNESTOCK, L. A., QUINN, D. D., MCFARLAND, D. M., SPENCER, B. F., VAKAKIS, A. F., and BERGMAN, L. A. Experimental testing and numerical simulation of a six-story structure incorporating two-degree-of-freedom nonlinear energy sink. *Journal of Structural Engineering*, **140**, 04014027 (2014)

[28] CHARLEMAGNE, S., LAMARQUE, C. H., and SAVADKOOHI, A. T. Vibratory control of a linear system by addition of a chain of nonlinear oscillators. *Acta Mechanica*, **228**, 3111–3133 (2017)

[29] GRINBERG, I., LANTON, V., and GENDELMAN, O. V. Response regimes in linear oscillator with 2DOF nonlinear energy sink under periodic forcing. *Nonlinear Dynamics*, **69**, 1889–1902 (2012)

[30] LEE, Y. S., VAKAKIS, A. F., BERGMAN, L. A., MCFARLAND, D. M., and KERSCHEN, G. Enhancing the robustness of aeroelastic instability suppression using multi-degree-of-freedom nonlinear energy sinks. *AIAA Journal*, **46**, 1371–1394 (2008)

[31] TAGHIPOUR, J. and DARDEL, M. Steady state dynamics and robustness of a harmonically excited essentially nonlinear oscillator coupled with a two-DOF nonlinear energy sink. *Mechanical Systems and Signal Processing*, **62-63**, 164–182 (2015)

[32] VAURIGAUD, B., SAVADKOOHI, A. T., and LAMARQUE, C. H. Targeted energy transfer with parallel nonlinear energy sinks. Part I: design theory and numerical results. *Nonlinear Dynamics*, **66**, 763–780 (2011)

[33] ZHANG, Y. W., ZHANG, Z., CHEN, L. Q., YANG, T. Z., FANG, B., and ZANG, J. Impulse-induced vibration suppression of an axially moving beam with parallel nonlinear energy sinks. *Nonlinear Dynamics*, **82**, 61–71 (2015)

[34] CHEN, J. E., HE, W., ZHANG, W., YAO, M. H., LIU, J., and SUN, M. Vibration suppression and higher branch responses of beam with parallel nonlinear energy sinks. *Nonlinear Dynamics*, **91**, 885–904 (2018)

[35] DING, H. and CHEN, L. Q. Designs, analysis, and applications of nonlinear energy sinks. *Nonlinear Dynamics*, **100**, 3061–3107 (2020)

[36] ZHANG, Y. W., XU. K. F., ZANG, J., NI, Z. Y., ZHU, Y. P., and CHEN, L. Q. Dynamic design of a nonlinear energy sink with NiTiNOL-steel wire ropes based on nonlinear output frequency response functions. *Applied Mathematics and Mechanics* (*English Edition*), **40**(6), 1791–1804 (2019) https://doi.org/10.1007/s10483-019-2548-9

[37] GENG, X. F., DING, H., WEI, K. X., and CHEN, L. Q. Suppression of multiple modal resonances of a cantilever beam by an impact damper. *Applied Mathematics and Mechanics* (*English Edition*), **41**(7), 383–400 (2020) https://doi.org/10.1007/s10483-020-2588-9

[38] XUE, J. R., ZHANG, Y. W., DING, H., and CHEN, L. Q. Vibration reduction evaluation of a linear system with a nonlinear energy sink under a harmonic and random excitation. *Applied Mathematics and Mechanics* (*English Edition*), **41**(7), 1–14 (2020) https://doi.org/10.1007/s10483-020-2560-6

[39] AHMADABADI, Z. N. Nonlinear energy transfer from an engine crankshaft to an essentially nonlinear attachment. *Journal of Sound and Vibration*, **443**, 139–154 (2019)

[40] TAGHIPOUR, J., DARDEL, M., and PASHAEI, M. H. Vibration mitigation of a nonlinear rotor system with linear and nonlinear vibration absorbers. *Mechanism and Machine Theory*, **128**, 586–615 (2018)

[41] TIAN, W., LI, Y. M., LI, P., YANG, Z. C., and ZHAO, T. Passive control of nonlinear aeroelasticity in hypersonic 3-D wing with a nonlinear energy sink. *Journal of Sound and Vibration*, **462**, 114942 (2019)

[42] YANG, K., ZHANG, Y. W., DING, H., and CHEN, L. Q. Nonlinear energy sink for whole-spacecraft vibration reduction. *Journal of Vibration and Acoustics*, **139**, 021011 (2017)

[43] YANG, T. Z., LIU, T., TANG, Y., HOU, S., and LV, X. F. Enhanced targeted energy transfer for adaptive vibration suppression of pipes conveying fluid. *Nonlinear Dynamics*, **97**, 1937–1944 (2019)

[44] ZHOU, K., XIONG, F. R., JIANG, N. B., DAI, H. L., YAN, H., WANG, L., and NI, Q. Nonlinear vibration control of a cantilevered fluid-conveying pipe using the idea of nonlinear energy sink. *Nonlinear Dynamics*, **95**, 1435–1456 (2019)

[45] CHEN, H. Y., MAO, X. Y., DING, H., and CHEN, L. Q. Elimination of multimode resonances of composite plate by inertial nonlinear energy sinks. *Mechanical Systems and Signal Processing*, **135**, 106383 (2020)

[46] HUANG, D. M., LI, R. H., and YANG, G. D. On the dynamic response regimes of a viscoelastic isolation system integrated with a nonlinear energy sink. *Communications in Nonlinear Science and Numerical Simulation*, **79**, 104916 (2019)

[47] LI, X., ZHANG, Y. W., DING, H., and CHEN, L. Q. Integration of a nonlinear energy sink and a piezoelectric energy harvester. *Applied Mathematics and Mechanics* (*English Edition*), **38**(7), 1019–1030 (2017) https://doi.org/10.1007/s10483-017-2220-6

[48] NUCERA, F., VAKAKIS, A. F., MCFARLAND, D. M., BERGMAN, L. A., and KERSCHEN, G. Targeted energy transfers in vibro-impact oscillators for seismic mitigation. *Nonlinear Dynamics*, **50**, 651–677 (2007)

[49] AHMADI, M., ATTARI, N. K. A., and SHAHROUZI, M. Structural seismic response mitigation using optimized vibro-impact nonlinear energy sinks. *Journal of Earthquake Engineering*, **19**, 193–219 (2015)

[50] WANG, J. J., WANG, B., LIU, Z. B., ZHANG, C., and LI, H. B. Experimental and numerical studies of a novel asymmetric nonlinear mass damper for seismic response mitigation. *Structural Control and Health Monitoring*, **27**, e2513 (2020)

[51] CHEN, Y. Y., QIAN, Z. C., ZHAO, W., and CHANG, C. M. A magnetic bi-stable nonlinear energy sink for structural seismic control. *Journal of Sound and Vibration*, **473**, 115233 (2020)